The rotational excitation of HCN and HNC by He: new insights on the HCN/HNC abundance ratio in molecular clouds

E. Sarrasin, D. Ben Abdallah, M. Wernli, A. Faure, J. Cernicharo, F. Lique

Monthly Notices
of the
ROYAL ASTRONOMICAL SOCIETY

Mon. Not. R. Astron. Soc. **404,** 518–526 (2010) doi:10.1111/j.1365-2966.2010.16312.x

The rotational excitation of HCN and HNC by He: new insights on the HCN/HNC abundance ratio in molecular clouds

E. Sarrasin,[1] D. Ben Abdallah,[2] M. Wernli,[3] A. Faure,[3] J. Cernicharo[4] and F. Lique[1,5]★

[1]*LOMC – FRE 3102, CNRS – Université du Havre, 25 rue Philippe Lebon, BP 540, 76058 Le Havre, France*
[2]*Laboratoire de Spectroscopie atomique, Moléculaire et applications, Faculté des Sciences Université Tunis el Manar, Tunis 1060, Tunisie*
[3]*Laboratoire d'Astrophysique de Grenoble, Université Joseph Fourier, CNRS UMR 5571, BP 53, 38041 Grenoble Cedex 09, France*
[4]*Department of Astrophysics, CAB, INTA–CSIC, Crta Torrejón a Ajalvir km 4, 28850 Torrejón de Ardoz, Spain*
[5]*LERMA and UMR 8112 of CNRS, Observatoire de Paris-Meudon, 92195 Meudon Cedex, France*

Accepted 2010 January 7. Received 2010 January 5; in original form 2009 October 31

ABSTRACT

Modelling of molecular emission from interstellar clouds requires the calculation of rates for excitation by collisions with the most abundant species. The present paper focuses on the calculation of rate coefficients for rotational excitation of the hydrogen cyanide (HCN) and hydrogen isocyanide (HNC) molecules in their ground vibrational state in collision with He. The calculations are based on new two-dimensional potential energy surfaces obtained from highly correlated *ab initio* calculations. Calculations of pure rotational (de)excitation cross-sections of HCN and HNC by He were performed using the essentially exact close-coupling method. Cross-sections for transitions among the eight first rotational levels of HCN and HNC were calculated for kinetic energies up to 1000 cm^{-1}. These cross-sections were used to determine collisional rate constants for temperatures ranging from 5 to 100 K. A propensity for even Δj transitions is observed in the case of HCN–He collisions whereas a propensity for odd Δj transitions is observed in the case of HNC–He collisions. The consequences for astrophysical models are evaluated and it is shown that the use of HCN rate coefficients to interpret HNC observations can lead to significant inaccuracies in the determination of the HNC abundance, in particular, in cold dark clouds for which the new HNC rates show that the $j = 1 - 0$ line of this species will be more easily excited by collisions than HCN. An important result of the new HNC–He rates is that the HNC/HCN abundance ratio derived from observations in cold clouds has to be revised from >1 to $\simeq 1$, in good agreement with detailed chemical models available in the literature.

Key words: molecular data – molecular processes – scattering.

1 INTRODUCTION

The isomers hydrogen cyanide (HCN) and hydrogen isocyanide (HNC) are among the most abundant organic molecules in space, from dark cold clouds (e.g. Irvine & Schloerb 1984) to circumstellar envelopes (e.g. Cernicharo et al. 1996), cool carbon stars (Harris et al. 2003), comets (e.g. Lis et al. 1997) and active galaxies (Pérez-Beaupuits, Aalto & Gerebro 2007). HCN and HNC also belong to the small class of molecules detected in high-redshift galaxies, along with CO, CN and HCO^+ (Guélin et al. 2007). In addition to thermal emission from various rotational transitions at (sub)millimetre and far-infrared wavelengths, a few masering lines have also been detected for both isomers (e.g. Lucas & Cernicharo 1989; Aalto et al. 2009). Thus, in contrast to purely thermochemical considerations (HNC is less stable than HCN by about 0.6 eV; Bowman et al. 1993), the abundance of HNC in space is large: the abundance ratio [HNC]/[HCN] is observed to vary from ∼1/100, e.g. in high-mass star-forming regions (Schilke et al. 1992), up to 4.5 in dark cold clouds (Hirota et al. 1998). The large variation of this ratio remains a puzzle in astrochemistry, although the major source of both isomers is thought to be the dissociative recombination of $HCNH^+$ with electrons (e.g. Amano et al. 2008, and references therein). Finally, we note that the HNC/HCN (rotational) line ratio is now employed to distinguish photon-dominated regions (PDR) and X-ray-dominated regions (XDR): PDR sources all have ratios lower than unity while XDR have ratios larger than 1 (Meijerink & Spaans 2005).

★E-mail: francois.lique@univ-lehavre.fr

Due to the low density of the interstellar medium ($\sim 10^5$ cm^{-3}), the rotational levels of molecules are generally not at local thermodynamic equilibrium. Reliable determination of molecular abundances therefore relies on accurate molecular collisional rates. Hydrogen molecules are generally the most abundant colliding partners in interstellar space, although collisions with H, He and free electrons can also play important roles in energetic regions. Rate coefficients for the rotational excitation of HCN by He atoms (employed as substitutes for H_2) have been calculated by Green & Thaddeus (1974), Green (unpublished)[1] and Monteiro & Stutzki (1986) (see also references therein). All these studies were based on the same potential energy surface (PES) obtained using the uniform electron gas model (Green & Thaddeus 1974). For HNC, there is to the best of our knowledge no collisional data except those of Faure et al. (2007) for electron-impact excitation. In astrophysical applications, HNC and HCN have been therefore assumed to present similar collisional rates (see, in particular, the discussion in Guélin et al. 2007). Similar HCN and HNC rotational rates were also observed for electron-impact excitation which is, however, dominated by the dipole interaction (Faure et al. 2007). In contrast, inelastic collisions between neutral species are dominated by short-range interactions and larger differences between HCN and HNC are expected.

In the present work, we present new rotational rate coefficients for HCN and HNC based on highly accurate, HCN−He and HNC−He PES. The paper is organized as follows. Section 2 describes the PES used in this work. Section 3 then contains a rapid description of the scattering calculations. In Section 4, we present and discuss our results. Finally, we analyse in Section 5 the effect of these new rate coefficients on the excitation of HCN and HNC by modelling this excitation through a large velocity gradient (LVG) code.

2 POTENTIAL ENERGY SURFACE

2.1 HCN–He

Several theoretical PES for the HCN–He system have been published during the last 15 yr [Drucker, Tao & Klemperer (1995); Atkins & Hutson (1996); Toczyłowski, Doloresco & Cybulski (2001), hereafter TDC01]. In the present study, we used the latter surface. As a reminder, it was computed *ab initio* using the single- and double-excitation coupled-cluster method (CCSD; Hampel, Peterson & Werner 1992) including perturbative contributions from connected triple excitations [CCSD(T)] computed as defined by Watts, Gauss & Bartlett (1993), with a triple zeta basis set and an additional [3s3p2d2f1g] set of bond functions (full details on the *ab initio* procedure used can be found in TDC01). The HCN molecule was treated as a linear rigid rotor with intramolecular distances fixed at the equilibrium values $r_{HC} = 2.013\,50$ bohr and $r_{CN} = 2.179\,23$ bohr (see discussion below in the case of HNC). The global minimum of this PES is in the linear He–HCN configuration at $R = 7.97$ bohr and has a well depth of 29.90 cm^{-1}.

A semi-empirical surface (Harada et al. 2002) is the latest PES published for HCN–He. It used the TDC01 surface as a starting point. The choice of the TDC01 surface seemed more adequate to us, as it is purely *ab initio* and thus consistent in the whole relevant interaction range, while the empirical PES used the measured spectrum of the bound van der Waals complex to refine the TDC01 surface in the region of the attractive well, thus possibly losing precision in other regions that could be as important for the present dynamical applications. A contour plot of the potential is shown in fig. 1 of TDC01.

The PES being strongly anisotropic due to the length of the HCN rod, we fitted the TDC01 surface with a Legendre polynomials basis

$$V(R,\theta) = \sum_{\lambda} V_\lambda(R) P_\lambda(\cos\theta), \quad (1)$$

using exactly the same truncation technique as for the HC_3N–He system in Wernli et al. (2007a,b). In this equation, R is the distance from the HCN centre of mass to the He atom, θ being the He–HCN angle as measured from the H side of HCN. The combination of 25 polynomials ($\lambda_{max} = 24$) and a cubic spline interpolation for the radial coefficients [$V_\lambda(R)$] was employed to obtain a precise fitting of the PES, the standard deviation between fitted and *ab initio* data being ≤ 1 cm^{-1} for all potential values lower than 300 cm^{-1}. We also tested our fit against the *ab initio* values given in the lower part of table I of TDC01 and found a difference ≤ 3 cm^{-1} for all 16 points in this table.

As a first outcome of the fitting, the V_λ with even λ were found to be significantly lower than those of Green & Thaddeus (1974) (table 3 in their article), indicating a lower (even) anisotropy of the TDC01 surface. This is expected to have an effect on the propensity rules, as shall be further discussed in Section 4.

2.2 HNC–He

To our knowledge, no PES exists for the HNC–He van der Waals system. The ground electronic state of the weakly bound HNC–He system is a singlet with A' refection symmetry. Within the ground electronic state, the equilibrium geometry of the HNC molecule is linear. Therefore, HNC can be considered as a linear rigid rotor. The HNC–He 'rigid rotor' PES is described by the two Jacobi coordinates R, the distance from the centre of mass of HNC to the He atom, and θ, the angle between $\boldsymbol{R}$ and the HNC bond axis $\boldsymbol{r}$, with $\theta = 0$ corresponding to colinear HeCNH. The HN and NC bond distances r_{HN} and r_{NC} were frozen at their experimental equilibrium value $r_{HN} = 1.8813$ bohr and $r_{NC} = 2.2103$ bohr (Huber & Herzberg 1979). As demonstrated by Lique & Spielfiedel (2007) for the CS–He system, for non-hydride diatomic molecules two-dimensional (2D) PES calculated for a frozen bond distance or obtained from full three-dimensional PES by averaging over the intermolecular ground state vibrational wavefunction are very similar. Consequently, in the present case, we anticipate that restricting r_{HN} and r_{NC} to their equilibrium value will introduce little error into the calculated inelastic rate coefficients.

The PES was calculated in the supermolecular approach at the CCSD(T) levels. The calculations were done with the MOLPRO 2006.1 package. For all three atoms, we used the standard correlation-consistent polarized valence-quadruple-zeta basis sets of Dunning (Dunning 1989) augmented with the diffuse functions of s, p, d, f and g symmetries by Kendall, Dunning & Harrison (1992). This basis set was further augmented by the [3s3p2d2f1g] bond functions optimized by Cybulski & Toczyłowski (1999) and placed at mid-distance between the He atom and the HNC centre of mass.

At all geometries, the Boys & Bernardi (1970) counterpoise procedure is used to correct for basis set superposition error. In this

[1] The earlier calculations of Green & Thaddeus (1974) (restricted to the lowest eight levels of HCN and temperatures of 5–100 K) were extended in 1993 to obtain rate constants among the lowest 30 rotational levels and for temperatures of 100–1200 K. These unpublished results are available at http://data.giss.nasa.gov/mcrates/#hcn.

procedure, the interaction energy is defined by

$$V(R,\theta) = E_{\mathrm{HNC-He}}(R,\theta) - E_{\mathrm{HNC}}(R,\theta) - E_{\mathrm{He}}(R,\theta), \quad (2)$$

where the energies of the HNC and He subsystems are determined with the full (four atoms plus bond functions) basis set.

Interaction energies at a total of 446 geometries were computed. The values of the radial scattering coordinate R ranged from 4 to 25 bohr. The angular grid was uniform with a 15° spacing from 0° to 180°. A contour plot of the potential is shown in Fig. 1. For this weakly bound system, the global minimum in the interaction energy was found to be -46.83 cm^{-1} ($R = 7.30$ bohr, $\theta = 180°$) corresponding to collinear He–HNC. We note the strong anisotropy of the PES.

The calculated interaction energies were fitted by means of the procedure described by Werner et al. (1989) for the CN–He system. The largest deviations between the fit and the *ab initio* points occur primarily in the repulsive region of the PES. Over the entire grid, the mean relative difference between the analytic fit and the *ab initio* calculations is 0.5 per cent. The dependence of the PES on the He–HNC angle was fitted by the usual Legendre expansion (equation 1). From an *ab initio* grid containing 13 values of θ, we were able to include terms up to $\lambda_{\max} = 12$.

The dependence on R of the dominant coefficients for the HCN–He and HNC–He PESs is shown in Fig. 2. We observe that, for the HCN–He system, the largest (in magnitude) of the anisotropic terms ($\lambda > 0$) corresponds to $\lambda = 2$. This implies that, to a first approximation, the PES is symmetric with respect to $\theta \rightarrow \pi - \theta$. At the opposite, for the HNC–He system, the largest of the anisotropic terms corresponds to $\lambda = 1$, 3 in the relevant range of R that is between 7 and 8 bohr. This reflects a large (odd) anisotropy for the PES. Consequences for the rotational excitation will be discussed in the next paragraph.

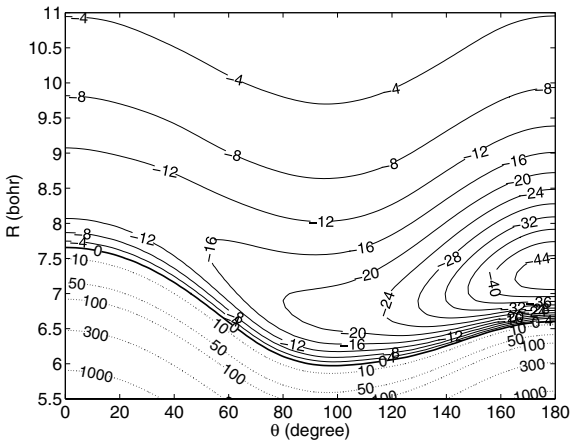

Figure 1. Contour plot of the 2D HNC–He PES as a function of R and θ. The energies are in cm^{-1} with the zero of energy taken to be HNC+He at infinite separation.

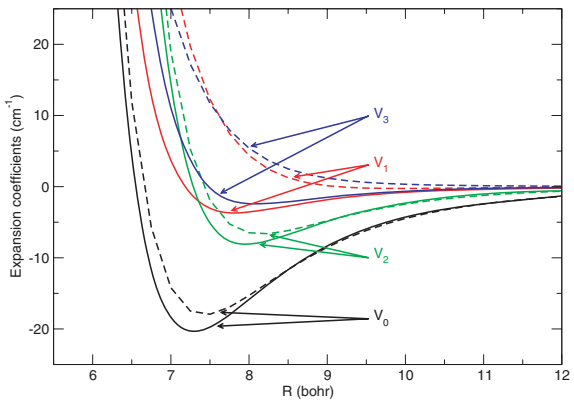

Figure 2. Plot of first four radial Legendre expansion coefficients ($\lambda = 0$–3) as a function of R. Solid lines denote HCN–He while dashed lines denote HNC–He.

3 DYNAMICAL CALCULATIONS

The main focus of this paper is the use of the two fitted HCN–He and HNC–He PESs to determine rotational excitation and de-excitation cross-sections of HCN and HNC molecules by He atoms. In the following, the rotational quantum number of HCN and HNC will be denoted by j. Despite the presence of a hyperfine structure in both molecules (Garvey & de Lucia 1974), we consider only the rotational structure of HCN and HNC.

To determine the inelastic cross-sections, we used the exact close-coupling (CC) approach of Arthurs & Dalgarno (1960). The integral cross-sections are obtained by summing the partial cross-sections over a sufficiently large number of values of the total angular momentum J until convergence is reached. The standard time-independent coupled scattering equations were solved using the MOLSCAT code (Hutson & Green 1994). Calculations were carried out at values of the total energy ranging from 3.2 to 1000 cm^{-1}. The integration parameters were chosen to ensure convergence of the cross-sections. We extended the rotational basis sufficiently to ensure convergence of the inelastic cross-sections. At the largest total energy considered (1000 cm^{-1}), the rotational basis was extended to $j = 14$ and 16, respectively, for the HCN–He and HNC–He calculations. The maximum value of the total angular momentum J used in the calculations was set large enough that the inelastic cross-sections were converged to within 0.005 Å^2.

From the rotationally inelastic cross-sections $\sigma_{j\rightarrow j'}(E_c)$, one can obtain the corresponding thermal rate coefficients at temperature T_K by an average over the collision energy (E_c):

$$k_{j\rightarrow j'}(T_K) = \left(\frac{8}{\pi\mu k_B^3 T_K^3}\right)^{1/2} \times \int_0^\infty \sigma_{j\rightarrow j'}(E_c)\, E_c\, \mathrm{e}^{\frac{-E_c}{k_B T}}\, \mathrm{d}E_c, \quad (3)$$

where μ is the reduced mass and k_B is Boltzmann's constant. To obtain precise values for the rate constants, the energy grid was chosen to be sufficiently fine to include the numerous scattering resonances which will be described below.

4 RESULTS

4.1 Cross-sections

Fig. 3 illustrates the typical energy dependence of the collisional de-excitation cross-sections obtained from the present CC calculations for a few selected rotational levels.

The de-excitation cross-sections are almost decreasing functions of the energy. For collision energies below 50 cm^{-1}, many resonances are found. These are a consequence of the quasi-bound states arising from tunnelling through the centrifugal energy barrier (shape resonances) or from the presence of an attractive potential well that allows the He atom to be temporarily trapped into the well and hence quasi-bound states to be formed (Feshbach resonances)

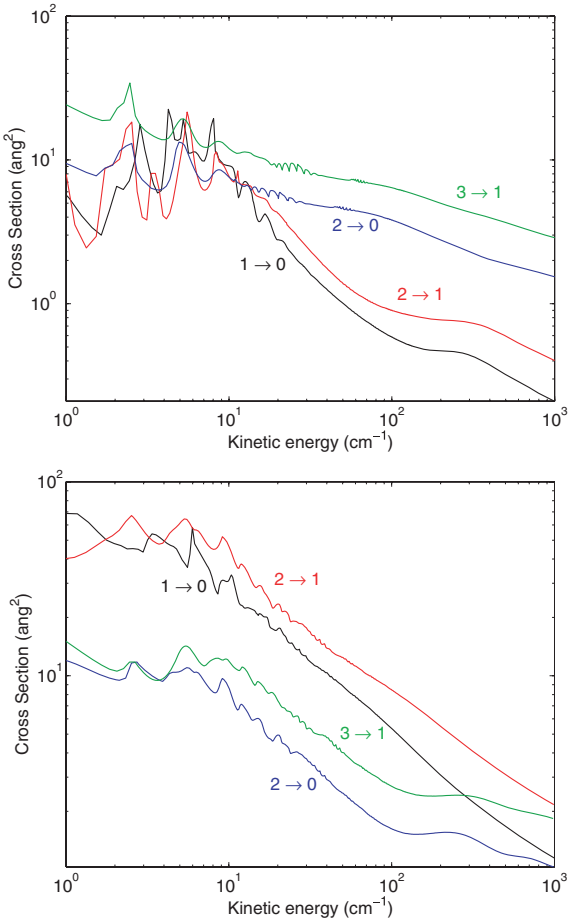

Figure 3. Typical rotational de-excitation cross-sections for the HCN (upper panel) and HNC (lower panel) molecules in collision with He as a function of the collision energy.

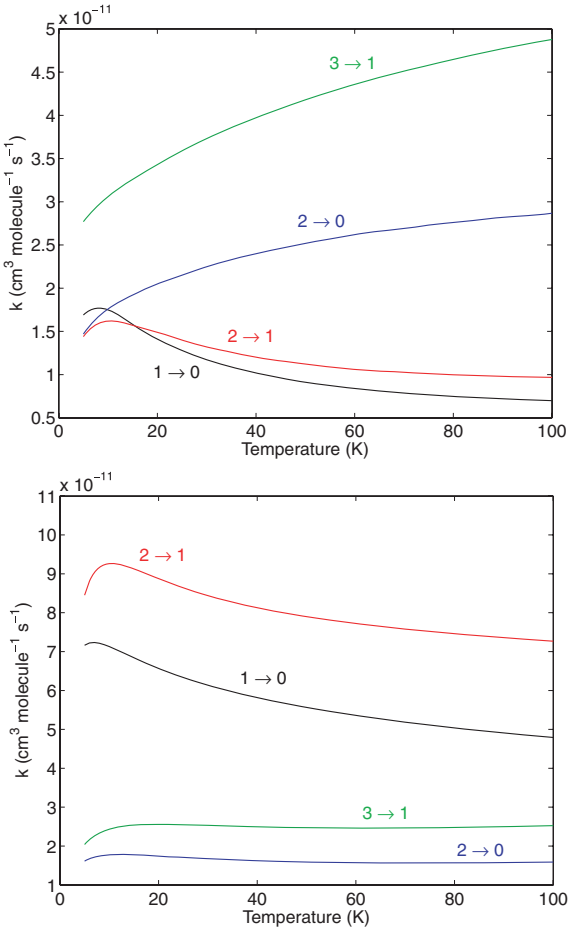

Figure 4. Typical rate coefficients for the HCN (upper panel) and HNC (lower panel) molecules in collision with He as a function of the temperature.

before the complex dissociates (Smith, Malik & Secrest 1979). Because of the averaging over collision energy (equation 3), these narrow resonances will have little, if any, effect on the relaxation rate coefficients.

4.2 Rate coefficients

We obtained, by energy averaging, de-excitation rate coefficients for the first eight ($j = 0$–7) rotational levels of HCN and HNC, from the CC cross-sections. The representative variation with temperature is illustrated in Fig. 4.

This complete set of (de)excitation rate coefficients is available online from the LAMDA[2] and BASECOL[3] websites. Excitation rate coefficients can be easily obtained by detailed balance:

$$k_{j\to j'}(T_K) = k_{j'\to j}(T_K)\frac{2j'+1}{2j+1}\exp[-(\varepsilon_{j'}-\varepsilon_j)/kT_K], \qquad (4)$$

where ε_j and $\varepsilon_{j'}$ are, respectively, the energies of the rotational levels j and j'.

As they are the only complete set of rotational rates available in the literature, astronomers still generally use the HCN–He rates of Green & Thaddeus (1974) in order to interpret HCN and HNC observations. Table 1 compares for selected transitions our HCN–He rates versus those of Green & Thaddeus (1974) at 10 and 100 K. We see that logically, the largest differences appear at low temperature. These differences can be attributed to the use of a new PES for the scattering calculations. The maximum difference at 100 K – the highest temperature for our data – is found on the smallest rate and is of a factor of 2. On the larger rates, the two sets match nearly.

Table 1. HCN–He and HNC–He rate coefficients at 10 and 100 K in 10^{-10} cm^3 mol^{-1} s^{-1}.

$j\,j'$	HCN	Green & Thaddeus (1974)	HNC
10 K			
1 0	0.175	0.110	0.817
2 0	0.176	0.241	0.203
3 0	0.005	0.012	0.058
4 0	0.021	0.045	0.026
100 K			
1 0	0.070	0.074	0.549
2 0	0.286	0.285	0.182
3 0	0.009	0.020	0.107
4 0	0.064	0.068	0.031

[2] http://www.strw.leidenuniv.nl/~moldata/
[3] http://basecol.obspm.fr/

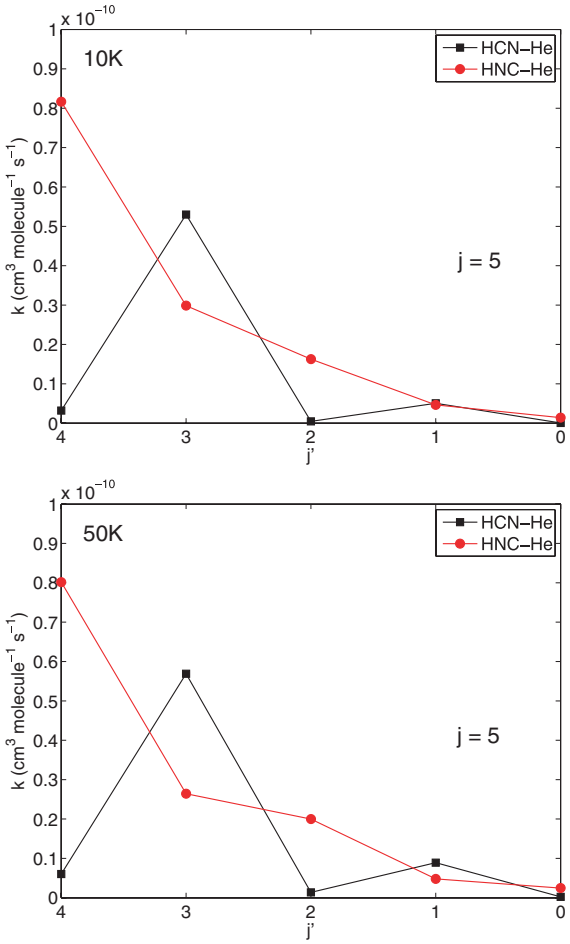

Figure 5. HCN–He and HNC–He de-excitation rate coefficients from the initial level $j = 5$ at 10 K (upper panel) and 50 K (lower panel).

4.3 Comparison between HCN and HNC rate coefficients

Fig. 5 shows the HCN–He and HNC–He de-excitation rate coefficients from the $j = 5$ level at 10 and 50 K.

One can see that significant differences exist between the HCN–He and HNC–He rate coefficients.

(i) Overall, the HNC rate coefficients seem to be larger than the HCN rate coefficients. This can be explained by a larger well depth of the HNC–He PES than the one of the HCN–He PES (46.83 versus 29.90 cm^{-1}).

(ii) The propensity rules seen in the two sets of rate coefficients are different. The HCN–He rate coefficients present a strong propensity in favour of transitions with even Δj whereas the HNC–He rate coefficients present a strong propensity in favour of transitions with odd Δj. These propensities are due to the shape of the PESs. Indeed, near-homonuclear symmetry of the PES, such as HCN–He PES, will favour transitions with even Δj whereas anisotropic PES, such as the HNC–He PES (see Fig. 2), will favour transitions with odd Δj (McCurdy & Miller 1977).

From this comparison, one can see that the use of HCN rate coefficients, in astrophysical applications, in order to interpret HNC observations may be dangerous since the use of 'real HNC rate coefficients' will probably significantly modify the excitation of the HNC molecule. This will be discussed in the next part.

5 ASTROPHYSICAL APPLICATIONS

5.1 HCN

We have estimated the line intensities of HCN using the present rate coefficients and compared the results with those obtained using the one of Green & Thaddeus (1974). Both sets of rates have been corrected for the different reduced mass of the system HCN–H_2, as molecular hydrogen is the main collision partner in molecular clouds:

$$k_{\mathrm{HCN\text{-}H_2}} = k_{\mathrm{HCN\text{-}He}} \left(\frac{\mu_{\mathrm{HCN\text{-}He}}}{\mu_{\mathrm{HCN\text{-}H_2}}} \right)^{1/2}, \quad (5)$$

where $\mu_{\mathrm{HCN--He}}$ and $\mu_{\mathrm{HCN\text{-}H_2}}$ are, respectively, the reduced mass of the HCN–He and HCN–H_2 collisional systems.

We have used an LVG code to derive excitation temperatures, opacities and brightness temperatures under different physical conditions. We have assumed a spherical cloud with an intrinsic linewidth of 1 $km\,s^{-1}$. We have selected three different temperatures: 10, 30 and 50 K, and the density has been varied from 10^2 to 10^9 cm^{-3}. The column densities of HCN had gone from 10^{12} (optically thin case) to 10^{15} cm^{-2} (very optically thick case). The results using the new rate coefficients are shown in Fig. 6 [solid lines; dashed lines are the results for HNC (see next section)] which can be used to estimate physical conditions of the gas from the observed intensities of the $j = 1 - 0$, $2 - 1$ and $3 - 2$ lines in astronomical objects.

In the optically thin case [$N(\mathrm{HCN}) \leq 10^{13} \mathrm{cm}^{-2}$] very high densities are needed to excite significantly the $j = 1 - 0$ line of HCN while in the optically thick case, the HCN excitation is dominated by radiative effects and strong emission could be obtained even in the case of densities $\leq 10^4$ cm^{-3}. For these large opacities and narrow

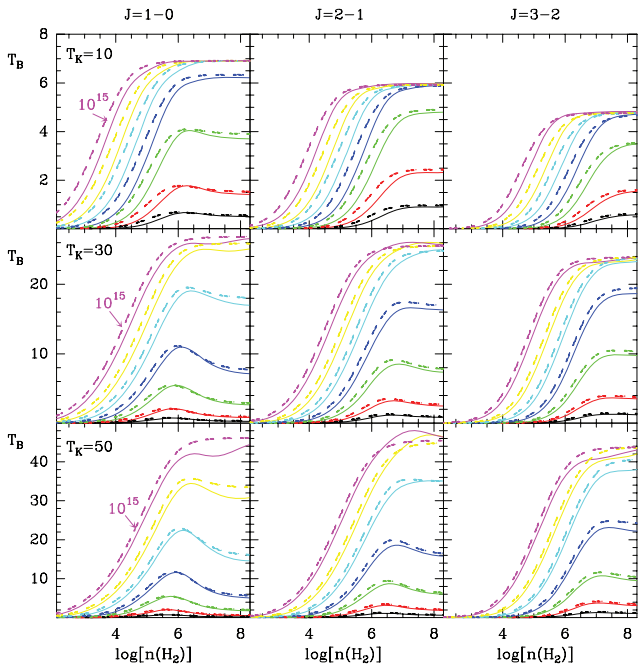

Figure 6. Solid lines: brightness temperature for the $j = 1 - 0$, $j = 2 - 1$ and $j = 3 - 2$ lines of HCN (indicated at the top of each column) derived using our new rate coefficients for temperatures of 10, 30 and 50 K (indicated in the left-hand panels). The column density varies between 10^{12} and 10^{15} cm^{-2} by steps of $10^{1/2}$ (see text). Brightness temperatures are in K and densities in cm^{-3}. Dashed lines: the same for HNC using the HNC–He rate coefficients obtained in this work.

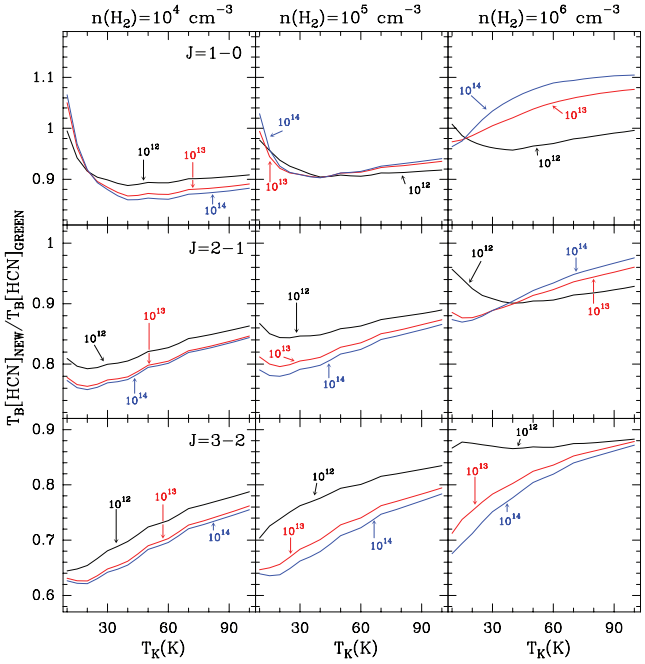

Figure 7. Ratio of the intensities of the $j = 1 - 0$, $j = 2 - 1$ and $j = 3 - 2$ lines of HCN (as indicated in the left-hand panels) using our new collisional HCN–He rate coefficients over those obtained from the rates of Green & Thaddeus (1974). Three densities, 10^4, 10^5 and 10^6 cm^{-3} have been considered as indicated in the top panels. We have considered three cases for the opacity of the $j = 1 - 0$ line : optically thin [N(HCN) = 10^{12} cm^{-2}], moderately thick [$\tau \simeq 1$, N(HCN) = 10^{13} cm^{-2}] and optically thick [N(HCN) = 10^{14} cm^{-2}]. The kinetic temperature varies between 10 and 100 K (see text).

lines, more sophisticated models taking into account the hyperfine structure of the molecule have to be performed to deal in detail with the radiative transfer of HCN (see Kwan & Scoville 1975; Guilloteau & Baudry 1981; Cernicharo et al. 1984; Cernicharo & Guelin 1987; González-Alfonso & Cernicharo 1993).

In order to compare our results with those obtained using the Green & Thaddeus (1974) rates, we show in Fig. 7 the ratio of the intensity for the $j = 1 - 0$, $j = 2 - 1$ and $j = 3 - 2$ lines obtained using the new rate coefficients and those derived using the previous ones, $R = T_B$(new)/T_B(old). Similar to the calculations described above, the number of rotational levels included in the calculations is 8 ($j = 0 - 7$). The temperature varies between 10 and 100 K, the highest temperature of the new and old HCN–He rate coefficients. We have considered three different column densities for HCN, 10^{12}, 10^{13} and 10^{14} cm^{-2}, which correspond for the $j = 1 - 0$ transition to the optically thin ($\tau < 1$), moderate optically thick ($\tau \simeq 1$), and optically thick ($\tau > 1$) cases, respectively. For the density, we have selected also three values, 10^4, 10^5 and 10^6 cm^{-3}, corresponding to low, moderate and high collisional excitation, respectively. As one could expect from a comparison of the rates given in Table 1, only small differences are found in the predicted intensity ratios. For the $j = 1 - 0$ line, we found similar intensities using both sets of collisional rates at low temperatures (a few percent difference for $T_K < 20$ K). The column density of HCN plays little effect in the low- and moderate-density cases. The largest differences for the $j = 1 - 0$ line are found for $n(H_2) = 10^6$ cm^{-3}. The situation is slightly different for the $j = 2 - 1$ and $j = 3 - 2$ lines. For low temperature, the intensity ratios obtained with both sets of rate coefficients show differences of 20 and 35 per cent, respectively, for low and moderate densities (10^4 and 10^5 cm^{-3}).

To further explore these effects, we have considered the following case: $T_K = 50$ K, n(H_2) = 10^5 cm^{-3} and N(HCN) = 10^{13}cm^{-2}. The old rate coefficients produce intensities for the $j = 1 - 0$, $j = 2 - 1$ and $j = 3 - 2$ lines of 3.6, 2.2 and 0.8 K, respectively. These intensities can be reproduced using the new rate coefficients for a density of 1.3 10^5 cm^{-3}. Hence, very small errors are introduced in the interpretation of the data using the Green & Thaddeus (1974) rate coefficients for warm molecular clouds. However, for $T_K = 10$ K the predicted intensities for these lines using the old rates is 1.56, 0.57 and 0.09 K, respectively. With the new rates they are 1.55, 0.45 and 0.057 K, respectively. The line intensity ratios $j = 1 - 0/j = 2 - 1$ and $j = 1 - 0/j = 3 - 2$ are different between both sets of rates while the $j = 2 - 1/j = 3 - 2$ intensity ratio is similar. Hence, the interpretation of astronomical observations of HCN using the old HCN–He rates will be difficult in some cases as it will be hard to fit the observed line intensity ratios. Consequently, we recommend the use of the new HCN–He rate coefficients in interpreting observed line intensities.

5.2 HNC

Rate coefficients for HNC with Helium (or H_2) have not been available until the present work. Interpretation of astronomical observations has been done using the HCN–He rate coefficients on the basis that the HNC–He and HCN–He PES could not be very different, that the dipole moment of both molecules differ by less than 3 per cent and that the energy levels for both species are similar. However, the comparison of both sets of rates done in previous sections indicates that some excitation effects could arise from the different propensity rules for both species and from the value of the $k_{0\rightarrow}$ 1 rate coefficients (see Table 1), which differs by a factor of $\simeq 5$ between both species. We have derived brightness temperatures for the HNC $j = 1 - 0, 2 - 1$ and $3 - 2$ lines using the rates calculated in this work for the same set of models than for HCN. The results are shown Fig. 6 (dashed lines). The excitation temperature of the $j = 1 - 0$ line of HNC is larger than that of HCN for the three temperatures considered in our calculations and for all column densities (abundances). The same applies to the $j = 2 - 1$ and $j = 3 - 2$ transitions for low temperature. However, the differences in predicted brightness temperatures for these two lines are less important for kinetic temperatures above 30 K. Hence, we have two different effects for HNC with respect to HCN.

(i) The $j = 1 - 0$ line will be, for identical physical conditions and molecular abundances, considerably stronger for HNC than for HCN, i.e. it is more easily excited which is a direct result of the larger collisional rates for HNC. The same applies to the $j = 2 - 1$ and $j = 3 - 2$ lines, but the effect is less pronounced.

(ii) The intensity line ratios will have significant differences for both molecules.

Therefore, the densities derived from astronomical observations of HNC and HCN could be different. Moreover, in the optically thin case the lines from these species could trace different areas of the cloud. Our calculations indicate that the $j = 1 - 0$ line of HNC could show weak maser effects for moderate column densities (low line opacities) and densities between 10^5 and 10^6 cm^{-3} for temperatures above 30 K (i.e. similar to the behaviour of the HCN $j = 1 - 0$ line). However, no population inversion, such as the one tentatively

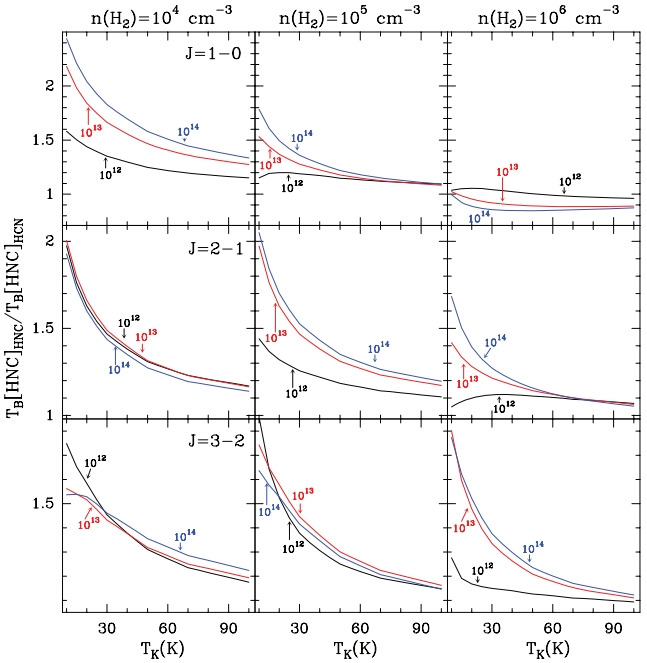

Figure 8. Ratio of the line intensities of the $j = 1 - 0, j = 2 - 1$ and $j = 3 - 2$ transitions of HNC (as indicated in the left-hand panels) obtained using our new collisional rates HNC–He over those obtained when the HCN–He rates are adopted for HNC. Three densities, 10^4, 10^5 and 10^6 cm^{-3}, have been considered as indicated in the top panels. We have considered three cases for the opacity of the $j = 1 - 0$ line at low kinetic temperature: optically thin [N(HNC) = 10^{12} cm^{-2}], moderately thick [$\tau \simeq 1$, N(HNC) = 10^{13} cm^{-2}] and optically thick [N(HNC) = 10^{14} cm^{-2}]. The kinetic temperature varies between 10 and 100 K (see text).

reported by Aalto et al. (2009) in the direction of Arp220, has been found for the $j = 3 - 2$ line.

In order to quantify the effect of the new rate coefficients on the excitation of the rotational levels of HNC, we have compared the line intensities obtained with the HNC–He rates and those obtained when the HCN–He rates are adopted for HNC. Fig. 8 shows the intensity ratio $R = T_B(j \rightarrow j - 1)$[HNC-He]/$T_B(j \rightarrow j - 1)$[HCN-He] for the $j = 1 - 0, 2 - 1$ and $3 - 2$ transitions. Three different column densities have been considered: 10^{12}, 10^{13} and 10^{14} cm^{-2} (optically thin, $\tau \simeq 1$, and optically thick, respectively). The volume density has been selected for the case of low, medium and high collisional excitation ($n(H_2) = 10^4, n(H_2) = 10^5$, and $n(H_2) = 10^6$ cm^{-3}, respectively). We see that the intensity ratios predicted by both sets of collisional rates approach unity for high temperature for all column densities. However, for low and moderate kinetic temperature there are significant differences in the derived brightness temperatures. The $j = 1 - 0$ transition is predicted up to 2.5 times stronger using the HNC–He rate coefficients than that obtained from the HCN–He ones. The effect is less prominent for the $j = 2 - 1$ transition and never exceeds 10 per cent for the $j = 3 - 2$ one. This behaviour has strong implications for the interpretation of the observations of HNC in cold dark clouds as the density required to obtain the same brightness temperature is lower for the HNC–He rates than for the HCN–He ones. Moreover, using the latter rates, it will be difficult to fit the line intensity ratios $R_{12} = T_B(1 - 0)/T_B(2 - 1)$, $R_{13} = T_B(1 - 0)/T_B B(3 - 2)$ and $R_{23} = T_B(2 - 1)/T_B(3 - 2)$. R_{12} has a value of $\geq$7 for all column densities, $n(H_2) \leq 10^4$ cm^{-2} and $T_K = 10$ K, using the HNC–He rates. Its value is $\simeq$5.5 using the HCN–He ones. R_{23} reaches a value of 17 with the HNC–He rates and of 14 with the HCN–He ones for the same range of physical conditions. For $n(H_2)$ larger than a few 10^6 cm^{-3}, the value of $R_{jj'}$[HNC–He]/$R_{jj'}$[HCN–He] approaches unity. For $T_K \geq 30$ K, the R_{23} ratio does not show any significant difference (below 20 per cent) between both sets of collisional rates. However, the R_{12} and R_{13} ratios still show important discrepancies for $n(H_2) \leq 10^5$ cm^{-3}.

As an example to quantify how important are these errors, one could consider a typical dark cloud with $n(H_2) = 10^4$ cm^{-3}, $T_K = 10$ K and N(HNC)=10^{13} cm^{-2}. To fit the predicted $j = 1 - 0$ line intensity from the HNC–He rates using the HCN–He ones, we will need to increase the column density of HNC by a factor of 2.4. Consequently, it seems obvious that the HNC–He collisional rates have to be used over the HCN–He ones at least for low and moderate temperatures. Moreover, for low kinetic temperature the abundances of HNC reported in the literature have to be revised as the new rates indicated that the HNC abundance has probably been overestimated by a factor of 2–3 depending on the physical conditions of the cloud. It is particularly interesting to note that the $j = 1 - 0$ line of HNC, being more easily excited than that of HCN, could be formed in zones of the cloud different from those of HCN.

The large different collisional excitation between the $j = 1 - 0$ line of HNC and HCN has important consequences for the chemical modelling of dark clouds. Irvine & Schloerb (1984) pointed out the need for an HNC/HCN abundance ratio >1 in these objects. Many other authors have arrived to the same conclusion. However, from a detailed modelling, Herbst, Terzieva & Talbi (2000) concluded that, from a chemical point of view, it was not possible to reproduce the derived abundances in dark clouds and that the HNC/HCN abundance ratio could not be very different from unity at $T_K =$ 10 K. The present results provide an explanation to this observational problem and allow us to conclude that in cold dark clouds the HNC/HCN abundance ratio is $\simeq$1.

For $T_K \geq 100$ K, it appears from Fig. 8 that the HCN–He collisional rates will produce reasonable results in interpreting the observed HNC line intensities and line intensity ratios. Hence, the relative abundances between both species derived in the literature towards warm molecular clouds are not significantly affected by the use of these rates.

6 SUMMARY AND CONCLUSION

We have used quantum scattering calculations to investigate rotational energy transfer in collisions of HCN and HNC molecules with He atoms. The calculations are based on new, highly accurate 2D PESs. Rate coefficients for transitions involving the lowest eight levels of these molecules were determined for temperatures ranging from 5 to 100 K. Strong propensity rule for even Δj was found in the case of HCN–He system whereas propensity rules for odd Δj were found in the case of HNC–He system.

The impact of these new rate coefficients on astrophysical modelling has been evaluated. The new HCN–He collisional rates have little impact on the interpretation of observations for warm and hot molecular clouds as the use of the previous rates (Green & Thaddeus 1974) produce line intensities that differ from those obtained from our rates by an amount similar to the calibration accuracy of radio observations in the millimetre and submillimetre domains. However, for low kinetic temperature, the previous collisional rates could not reproduce the observed line intensity ratios $j = 1 - 0/j = 2 - 1$ and $j = 1 - 0/j = 3 - 2$. For $T_K < 100$ K, we recommend to use our rates. The situation is different for HNC as

no previous collisional rates are available and the interpretation of astronomical observations has been based on the use of the Green & Thaddeus (1974) rates for HCN. We have found significant variations in the predicted line intensities and line intensity ratios using the HNC–He rates instead of the HCN–He ones (our calculations for HCN). In particular, in cold dark clouds the interpretation of the HNC line intensities will dramatically suffer if the HCN–He rates are used rather than the correct HNC–He ones. The main collider in molecular clouds is however molecular hydrogen. Hence, these conclusions could be limited to the case of HCN/HNC–para-H_2 ($j = 0$) for which the collisional rates are expected to be very similar to those of HCN/HNC–He (see below).

Our results for HNC indicate that the HNC/HCN abundance ratio derived from observations towards dark clouds has to be revised. The best fit to the observations available in the literature is obtained for HNC/HCN $\simeq 1$. We have neglected in our calculations the hyperfine structure of HCN and HNC. Although difficult to spectroscopically resolve for the latter, for the former species the line intensities of the different hyperfine components are known to show important intensity anomalies (Kwan & Scoville 1975; Walmsley et al. 1982; Cernicharo et al. 1984; González-Alfonso & Cernicharo 1993), which can be explained as the result of their different opacities across the cloud (Cernicharo et al. 1984; Cernicharo & Guelin 1987; González-Alfonso & Cernicharo 1993). Line overlaps also play an important role in the excitation of HCN in molecular clouds (González-Alfonso & Cernicharo 1993). They are responsible of the strong masers found in other species (see e.g. Gonzalez-Alfonso, Alcolea & Cernicharo 1996; Gonzalez-Alfonso & Cernicharo 1997). Hence, a correct treatment of the radiative transfer of HCN (and in some cases also of HNC) in molecular clouds will require a detailed knowledge of the collisional rates between hyperfine components. These calculations are under development and will be published elsewhere.

Finally, as already said, the great abundance of H_2 in the interstellar medium makes this molecule the primary collision partner for any other species. It is generally assumed (Lique et al. 2008) that rate coefficients with He can provide a good estimate of rate coefficients for collision with para-H_2 ($j = 0$). This approximation postulates that collisional cross-sections with He and para-H_2(j=0) are equal, so that the rate coefficients differ only by a reduced mass factor of $\approx$1.4 arising from the thermal averaging (equation 3). Recent results on rotational excitation of CO (Wernli et al. 2006), SO (Lique et al. 2007) and SiS (Lique & Kłos 2008; Kłos & Lique 2008) have pointed out that rate coefficients for collisions with para-H_2 ($j = 0$) can be up to a factor of 3 larger or smaller than those for collisions with He, depending on the selected transition, but that the He rate coefficients scaled by a factor of 1.4 provide the correct order of magnitude of the H_2 ($j = 0$) rate coefficients.[4] Therefore, the present results should provide a reasonable first estimate of collisional rate coefficients for collisions of HCN and HNC with para-H_2 ($j = 0$). On the other hand, it may be unadvisable to use the present He rate coefficients as an estimate of the ortho-H_2 rate coefficients, since the He and ortho-H_2 rate coefficients usually differ significantly. Specific calculations with ortho-H_2 must be performed. Thus, it is crucial to extend the calculations, both of the PES and of the inelastic cross-sections, to the HCN–H_2 and HNC–H_2 systems.

In any case, the full set of rate coefficients presented here will enhance our ability to understand and interpret future HCN and HNC observations. Collisional rates when the hyperfine structure is considered can be obtained from the present results and the standard assumption that the rates will be proportional to the degeneracy of the final hyperfine state, or employing the more physical infinite order sudden (IOS) scaling method (Faure et al. 2007).

[4] We note, however, that much larger differences between He and para-H_2 ($j = 0$) have been observed for small hydride molecules like H_2O (Dubernet et al. 2009) and NH_3 (Maret et al. 2009). However, detailed calculations by Cernicharo et al. (2009) indicate very little differences in the water vapour predictions in protoplanetary discs using H_2O–He and H_2O–H_2 ($j = 0$) collisional rates.

ACKNOWLEDGMENTS

FL and AF acknowledge the CNRS national programme 'Physique et Chimie du Milieu Interstellaire' for supporting this research. JC would like to thank the Spanish Ministerio de Ciencia e Innovacion for funding support through grants AYA2006-14876 and the DGU of the Madrid community government under IV-PRICIT project S-0505/ESP-0237 (ASTROCAM).

REFERENCES

Aalto S., Wilner D., Spaans M., Wiedner M. C., Sakamoto K., Black J. H., Caldas M., 2009, A&A, 493, 481
Amano T., Zelinger Z., Hirao T., Takano J., Toyoda R., 2008, J. Mol. Spectrosc., 251, 252
Arthurs A. M., Dalgarno A., 1960, Proc. R. Soc. Lond., Ser. A, 256, 540
Atkins K. M., Hutson J. M., 1996, J. Chem. Phys., 105, 440
Bowman J. M., Gazdy B., Bentley J. A., Lee T. J., Dateo C. E., 1993, J. Chem. Phys., 99, 308
Boys S. F., Bernardi F., 1970, Mol. Phys., 19, 553
Cernicharo J., Guelin M., 1987, A&A, 176, 299
Cernicharo J., Castets A., Duvert G., Guilloteau S., 1984, A&A, 139, L13
Cernicharo J. et al., 1996, A&A, 315, L201
Cernicharo J., Ceccarelli C., Ménard F., Pinte C., Fuente A., 2009, ApJ, 703, L123
Cybulski S. M., Toczyłowski R., 1999, J. Chem. Phys., 111, 10520
Drucker S., Tao F.-M., Klemperer W., 1995, J. Phys. Chem., 99, 2646
Dubernet M., Daniel F., Grosjean A., Lin C. Y., 2009, A&A, 497, 911
Dunning T. H., 1989, J. Chem. Phys., 90, 1007
Faure A., Varambhia H. N., Stoecklin T., Tennyson J., 2007, MNRAS, 382, 840
Garvey R. M., de Lucia F. C., 1974, J. Mol. Spectrosc., 50, 38
González-Alfonso E., Cernicharo J., 1993, A&A, 279, 506
Gonzalez-Alfonso E., Cernicharo J., 1997, A&A, 322, 938
Gonzalez-Alfonso E., Alcolea J., Cernicharo J., 1996, A&A, 313, L13
Green S., Thaddeus P., 1974, ApJ, 191, 653
Guélin M. et al., 2007, A&A, 462, L45
Guilloteau S., Baudry A., 1981, A&A, 97, 217
Hampel C., Peterson K. A., Werner H.-J., 1992, Chem. Phys. Lett., 190, 1
Harada K., Tanaka K., Tanaka T., Nanbu S., Aoyagi M., 2002, J. Chem. Phys., 117, 7041
Harris G. J., Pavlenko Y. V., Jones H. R. A., Tennyson J., 2003, MNRAS, 344, 1107
Herbst E., Terzieva R., Talbi D., 2000, MNRAS, 311, 869
Hirota T., Yamamoto S., Mikami H., Ohishi M., 1998, ApJ, 503, 717
Huber K. P., Herzberg G., 1979, Molecular Spectra and Molecular Structure. IV. Constants of Diatomic Molecules. Van Nostrand Reinhold, New York
Hutson J. M., Green S., 1994, MOLSCAT Computer Code, version 14
Irvine W. M., Schloerb F. P., 1984, ApJ, 282, 516
Kendall R. A., Dunning T. H., Harrison R. J., 1992, J. Chem. Phys., 96, 6796
Kłos J., Lique F., 2008, MNRAS, 390, 239
Kwan J., Scoville N., 1975, ApJ, 195, L85
Lique F., Kłos J., 2008, J. Chem. Phys., 128, 034306
Lique F., Spielfiedel A., 2007, A&A, 462, 1179

Lique F., Senent M.-L., Spielfiedel A., Feautrier N., 2007, J. Chem. Phys., 126, 164312
Lique F., Toboła R., Kłos J., Feautrier N., Spielfiedel A., Vincent L. F. M., Chałasiński G., Alexander M. H., 2008, A&A, 478, 567
Lis D. C. et al., 1997, Icarus, 130, 355
Lucas R., Cernicharo J., 1989, A&A, 218, L20
McCurdy C. W., Miller W. H., 1977, J. Chem. Phys., 67, 2488
Maret S., Faure A., Scifoni E., Wiesenfeld L., 2009, MNRAS, 399, 425
Meijerink R., Spaans M., 2005, A&A, 436, 397
Monteiro T. S., Stutzki J., 1986, MNRAS, 221, 33P
Pérez-Beaupuits J. P., Aalto S., Gerebro H., 2007, A&A, 476, 177
Schilke P., Walmsley C. M., Pineau Des Forets G., Roueff E., Flower D. R., Guilloteau S., 1992, A&A, 256, 595
Smith L. N., Malik D. J., Secrest D., 1979, J. Chem. Phys., 71, 4502
Toczyłowski R. R., Doloresco F., Cybulski S. M., 2001, J. Chem. Phys., 114, 851 (TDC01)
Walsmley C. M., Churchwell E., Nash A., Fitzpatrick E., 1982, A&A, 258, L75
Watts J. D., Gauss J., Bartlett R. J., 1993, J. Chem. Phys., 98, 8718
Werner H.-J., Follmeg B., Alexander M. H., Lemoine D., 1989, J. Chem. Phys., 91, 5425
Wernli M., Valiron P., Faure A., Wiesenfeld L., Jankowski P., Szalewicz K., 2006, A&A, 446, 367
Wernli M., Wiesenfeld L., Faure A., Valiron P., 2007a, A&A, 464, 1147
Wernli M., Wiesenfeld L., Faure A., Valiron P., 2007b, A&A, 475, 391

This paper has been typeset from a TEX/LATEX file prepared by the author.